11-7-2017

ROS Control Mitochondrial Motility through p38 and the Motor Adaptor Miro/Trak.

Valentina Debattisti
Thomas Jefferson University

Akos A. Gerencser
Buck Institute for Research on Aging

Masao Saotome
Thomas Jefferson University

Sudipto Das
Thomas Jefferson University

György Hajnóczky
Thomas Jefferson University

Cell Reports

Article

ROS Control Mitochondrial Motility through p38 and the Motor Adaptor Miro/Trak

Graphical Abstract

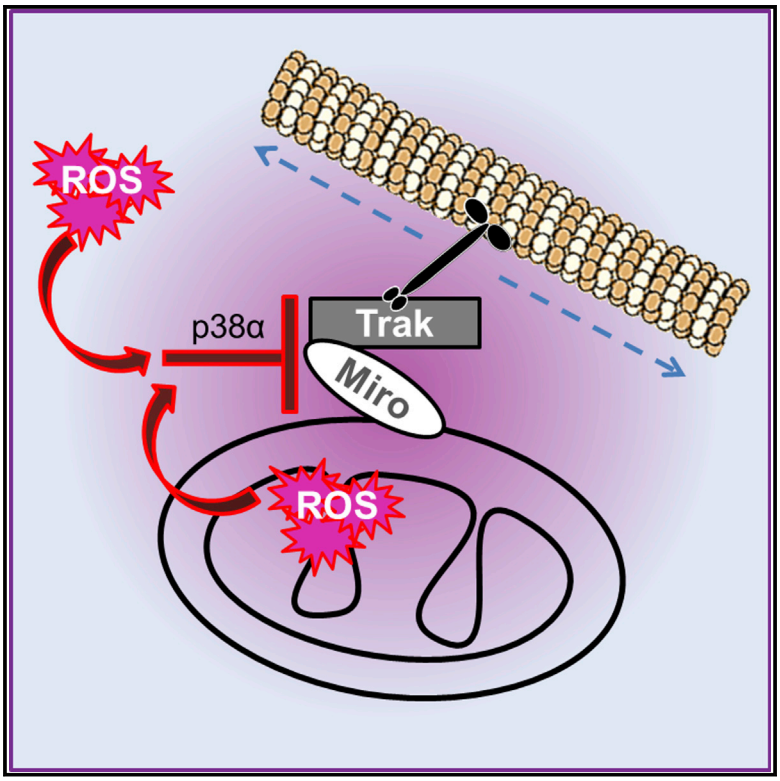

Authors

Valentina Debattisti, Akos A. Gerencser, Masao Saotome, Sudipto Das, György Hajnóczky

Correspondence

gyorgy.hajnoczky@jefferson.edu

In Brief

Debattisti et al. examine how reactive oxygen species induce dose-dependent and reversible arrest of mitochondrial motility independently of $[Ca^{2+}]_c$ in two different mammalian models. The authors argue that ROS target the adaptor complex through p38α to decrease mitochondrial movements.

Highlights

- ROS induce a reversible decrease in mitochondrial motility
- ROS-induced motility decrease is triggered independently of $[Ca^{2+}]_c$
- ROS-induced motility decrease does not require PTP opening or $\Delta\Psi_m$ dissipation
- p38α and the motor adaptor complex are required for ROS control of motility

Debattisti et al., 2017, Cell Reports *21*, 1667–1680
November 7, 2017
https://doi.org/10.1016/j.celrep.2017.10.060

Cell Reports
Article

ROS Control Mitochondrial Motility through p38 and the Motor Adaptor Miro/Trak

Valentina Debattisti,[1,3] Akos A. Gerencser,[2,3] Masao Saotome,[1,3] Sudipto Das,[1] and György Hajnóczky[1,4,*]
[1]MitoCare Center for Mitochondrial Imaging Research and Diagnostics, Department of Pathology, Anatomy and Cell Biology, Thomas Jefferson University, Philadelphia, PA, USA
[2]Buck Institute for Research on Aging, Novato, CA, USA
[3]These authors contributed equally
[4]Lead Contact
*Correspondence: gyorgy.hajnoczky@jefferson.edu
https://doi.org/10.1016/j.celrep.2017.10.060

SUMMARY

Mitochondrial distribution and motility are recognized as central to many cellular functions, but their regulation by signaling mechanisms remains to be elucidated. Here, we report that reactive oxygen species (ROS), either derived from an extracellular source or intracellularly generated, control mitochondrial distribution and function by dose-dependently, specifically, and reversibly decreasing mitochondrial motility in both rat hippocampal primary cultured neurons and cell lines. ROS decrease motility independently of cytoplasmic [Ca^{2+}], mitochondrial membrane potential, or permeability transition pore opening, known effectors of oxidative stress. However, multiple lines of genetic and pharmacological evidence support that a ROS-activated mitogen-activated protein kinase (MAPK), p38α, is required for the motility inhibition. Furthermore, anchoring mitochondria directly to kinesins without involvement of the physiological adaptors between the organelles and the motor protein prevents the H_2O_2-induced decrease in mitochondrial motility. Thus, ROS engage p38α and the motor adaptor complex to exert changes in mitochondrial motility, which likely has both physiological and pathophysiological relevance.

INTRODUCTION

Mitochondrial distribution and transport are central to many cellular functions, including cell differentiation (Chada and Hollenbeck, 2004), cell division to ensure proper inheritance (Yaffe, 1999), ATP supply at the local sites of demand, and Ca^{2+} buffering for intracellular Ca^{2+} homeostasis (Yi et al., 2004; Zucker, 1999). Strategic intracellular mitochondrial distribution depends on the movement of mitochondria, which is mediated by a complex of proteins first identified in genetic screens performed in *Drosophila melanogaster*. The anterograde mitochondrial transport in axons is abolished in either *Milton* or *Miro* mutants (Guo et al., 2005; Stowers et al., 2002); Milton co-immunoprecipitates with and attaches kinesin to mitochondria through Miro, an outer mitochondrial membrane (OMM) protein (Glater et al., 2006). In mammals, mitochondrial motility is mediated by trafficking kinesin proteins (Trak1 and Trak2, Milton homologs) that work as adaptors between Miro1 and Miro2 (Miro homologs) and dynein and kinesin motor proteins to allow movement of the organelles along the microtubules (Brickley et al., 2005; Fransson et al., 2006; Hirokawa et al., 1991; MacAskill et al., 2009a; Nguyen et al., 2014).

In the last decade, the mitochondrial motility machinery has been determined, but the signaling mechanisms underlying the specificity and the spatio-temporal control of the mitochondrial movements remained elusive. Mitochondrial membrane potential ($\Delta\psi_m$) is central to mitochondrial movement because agents that depolarize mitochondria inhibit mitochondrial transport (Rintoul et al., 2003; Vanden Berghe et al., 2004; Yi et al., 2004). First, mitochondria with high $\Delta\psi_m$ were shown to preferentially move anterogradely while depolarized ones move retrogradely (Miller and Sheetz, 2004), but later studies showed no directionality difference between the two populations (Gerencser et al., 2008; Verburg and Hollenbeck, 2008). Changes in ATP/ADP likely affect movements because ADP slowly dissociates from the motor to act like an inhibitor. We and others previously showed that motility is regulated by the cytoplasmic Ca^{2+} concentration ($[Ca^{2+}]_c$), providing the basis for a homeostatic circuit in which the organelles decrease their movements along microtubules at the sites of high $[Ca^{2+}]_c$ to locally buffer Ca^{2+} and contribute to ATP supply (Brough et al., 2005; Rintoul et al., 2003; Yi et al., 2004). Ca^{2+} sensing involves the helix-loop-helix structural domain (EF) hands of the Miro proteins (MacAskill et al., 2009b; Saotome et al., 2008; Wang and Schwarz, 2009).

Mitochondria are also a major site for production and scavenging of reactive oxygen species (ROS) that serve as both a mediator and a regulator of calcium signaling and are relevant for the control of mitochondrial function. Numerous studies have described ROS-induced changes in mitochondrial shape and distribution (Das et al., 2012; De Vos et al., 2007; Fang et al., 2012; Magrané et al., 2014; Morfini et al., 2013), but these changes can result from a variety of different mechanisms, and the effect of ROS on mitochondrial movements has not been addressed yet.

Here, we tested the hypothesis that ROS target motility to control mitochondrial dynamics. Alteration of mitochondrial distribution can be detrimental for several tissues, in particular for

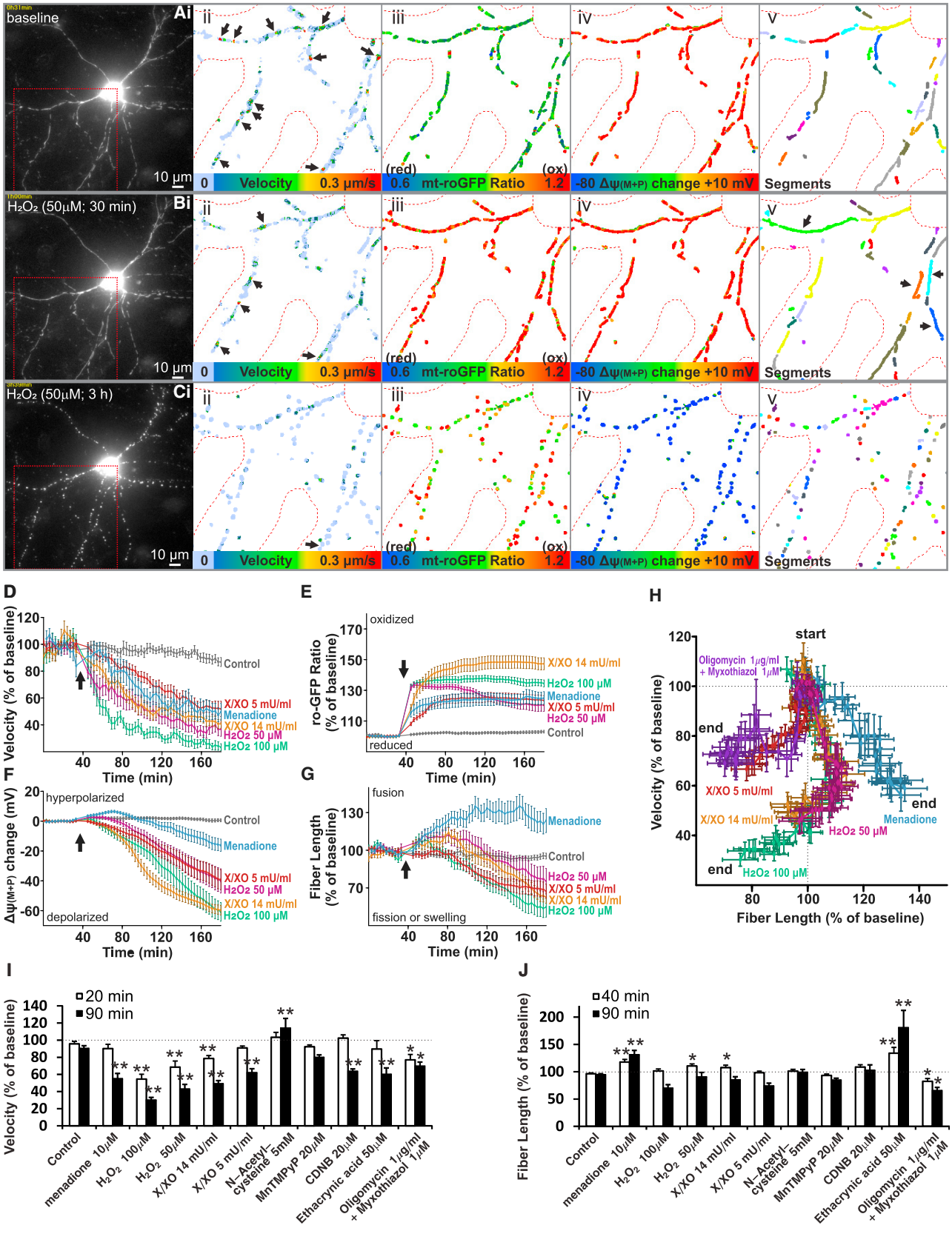

(legend on next page)

neurons, where impairments of mitochondrial transport machinery result in neurological deficits (Guo et al., 2005; Mattson et al., 2008; Nguyen et al., 2014) likely as a consequence of less efficient ATP supply and Ca^{2+} buffering in cell subdomains where organelles are lacking. We show that ROS exert a regulatory effect on mitochondrial motility. In both rat hippocampal neurons and cell lines (H9c2 cells and mouse embryonic fibroblasts [MEFs]), either external addition or intracellular generation of ROS decreases mitochondrial motility. The mechanism is dose dependent, reversible, and does not require permeability transition pore (PTP) opening or $\Delta\psi_m$ dissipation. In addition, this effect can occur independent of $[Ca^{2+}]_c$. However, both chemical and genetic targeting of p38α protects from the decrease in mitochondrial movements induced by H_2O_2. Furthermore, anchoring mitochondria directly to kinesins without involvement of the physiological adaptors between the organelles and the motor protein prevents the H_2O_2-induced decrease in motility, indicating that ROS likely target the adaptor complex with the involvement of p38α to control motility of mitochondria.

RESULTS

ROS Induce a Decrease in Mitochondrial Transport in Neurons

To assess a possible role of ROS in the control of mitochondrial motility in neurons, we assayed the effects of H_2O_2, menadione, and $O_2\bullet^-$ in mito-roGFP1-transfected rat hippocampal neurons (Figures 1Ai and S1Bi). The redox cycling compound menadione is a single electron reduced by ubiquinone in the inner mitochondrial membrane and subsequently reduces O_2, resulting in $O_2\bullet^-$ and H_2O_2 (Eklöw et al., 1981); therefore, it was used to aggravate endogenous ROS production. A multiplexed assay (Gerencser and Nicholls, 2008) was applied to follow mitochondrial transport velocities, length, SH redox status of mito-roGFP1, and $\Delta\Psi_M$ (Figure 1Aii–v). Velocities were measured using optical flow and also visualized by kymograms (Figure S1A). To quantify motility, we averaged optical flow for all visible neurites for each observed neuron. Importantly, this approach allowed a low rate of imaging at 5 min intervals to minimize photoillumination-induced effects and to record multiple view fields cyclically, while velocities were calculated from a pair of frames recorded at each time point.

Both H_2O_2 (50 μM) and menadione (10 μM) triggered simultaneous oxidation of roGFP and a decrease in the mitochondrial motility (Figures 1A–1G; Figures S1A–S1E). Increasing H_2O_2 to 100 μM induced both higher oxidation and inhibition of mitochondrial velocity. When $O_2\bullet^-$ (generated by 5–14 mU/mL xanthine oxidase with 100 μM xanthine [X/XO]) was used as an oxidant, a decrease in motility was also observed (Figures 1D and 1I). Treatment with X/XO had a strong oxidative property (Figure 1E) but was less effective than H_2O_2 in inhibiting mitochondrial transport. To control for cell viability, we measured plasma membrane potential ($\Delta\Psi_p$) in separate experiments by an anionic plasma membrane potential indicator (PMPI) (Nicholls, 2006) and intracellular $[Ca^{2+}]$ by rhod2 (under our conditions, rhod2 compartmentalized mostly to the cytoplasm) (Figures S1G and S1H). $\Delta\Psi_p$ did not depolarize in the first 2 hr of the exposure to H_2O_2 (100 μM) and menadione (10 μM). $[Ca^{2+}]_c$ did not elevate for 90 min in the presence of H_2O_2, while it slightly but gradually increased with menadione.

Inhibition of Mitochondrial Motility and Mitochondrial Elongation Induced by ROS Are Triggered Independently

Mitochondrial fusion-fission dynamics and movements are mutually coupled (Liu et al., 2009; Mouli et al., 2009). The motility decrease caused by H_2O_2 and $O_2\bullet^-$ was accompanied by elongation of neuronal mitochondria (Figures 1Bv, 1G, and 1J), which then underwent fragmentation, swelling, and membrane depolarization [$\Delta\Psi_{(m+p)}$; a surrogate for $\Delta\Psi_m$; Figures 1C, 1F, and 1G]. The elongation effect of ROS on mitochondrial morphology we observed was reproduced for all of the oxidants used, but not for all concentrations and with some differences in the temporal scale (Figures 1G and 1J). Notably, cells rapidly convert $O_2\bullet^-$ to H_2O_2 by superoxide dismutases, which is then removed by catalase and the glutathione system. Menadione and glutathione depletion instead induced a prolonged mitochondrial elongation, which was observed even after 2 hr from the addition of the drug. Mitochondria appearing visually elongated were also luminally continuous as indicated by spatially synchronous fluctuations of $\Delta\Psi_m$, best observable in neurons in the glutathione-depleted conditions with 1-chloro-2,4-dintrobenzene (CDNB) or ethacrynic acid (see below; Figure S1I). In contrast to shape changes, the inhibitory effect on mitochondrial motility was universal and early for H_2O_2, X/XO, and menadione treatments for all used concentrations.

To investigate the temporal relationship of the loss of motility, shape changes, and $\Delta\Psi_m$, we plotted the parameters shown in Figures 1D, 1F, and 1G against each other pairwise (Figure 1H; Figures S1J and S1K). In Figure 1H, the measured properties gradually deviate from the baseline ("start," 100% velocity and length) as the experiment progresses to the "end" (t = 120 min). H_2O_2 (50–100 μM) and X/XO (14 mU/mL) treatments resulted in a characteristic track in the velocity-length

Figure 1. ROS Decrease Mitochondrial Transport Velocity in Neurons (See Also Figure S1)

(A–C) A hippocampal neuron expressing mito-roGFP1 loaded in the presence of tetramethylrhodamine, methyl ester (TMRM) at time point 0 (baseline, Ai), 30 min (Bi), and 3 hr (Ci) after treatment with H_2O_2. Velocities of mitochondria (measured as optical flow, ii; arrows, motile mitochondria), redox state of mito-roGFP (expressed as 438/480 fluorescence ratio, iii), and changes in $\Delta\Psi_{M+P}$ (iv) are shown. The mito-roGFP image was also segmented to measure the length of mitochondria (v; arrows indicate fused mitochondria). The red quadrangle in (i) corresponds to (ii)–(v), and the red dashed outline in (ii)–(v) to a hand-drawn region of the analysis.

(D–G) Time courses of velocities (D), redox state of mito-roGFP1 (E), $\Delta\Psi_{M+P}$ (F), and mitochondrial length (fiber length) (G). The indicated treatments were present from t = 40 min. Mock-treated cells (control, gray trace) are shown.

(H) Parametric plot of velocity and mitochondrial length for the indicated treatments using data from (D) and (G).

(I and J) Mean velocities (I) and mitochondrial length (J) at the indicated time after application of the indicated treatments in mito-roGFP1-expressing rat hippocampal neurons. *$p < 0.05$; **$p < 0.01$.

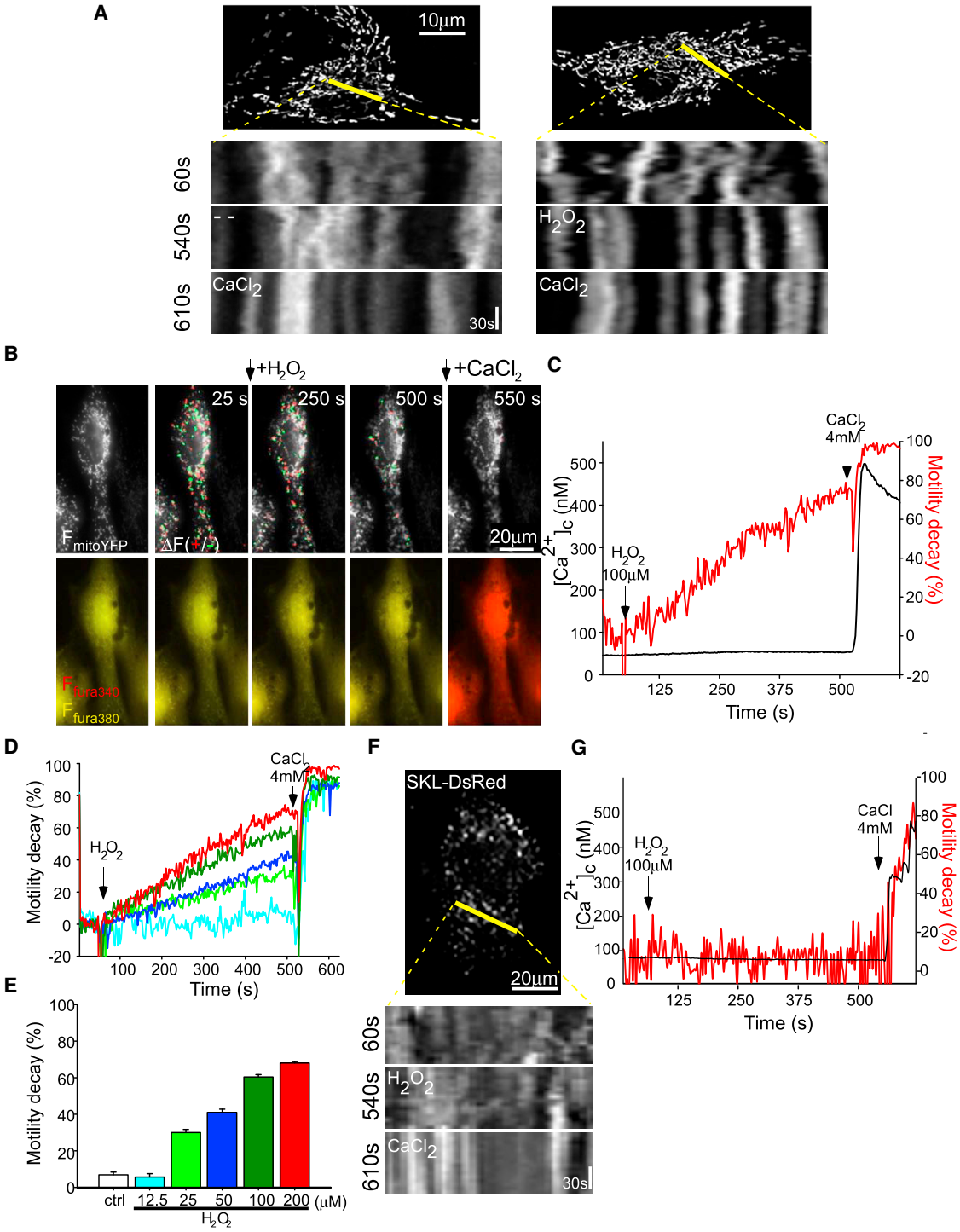

Figure 2. H_2O_2 Induces Mitochondrial Motility Inhibition in H9c2 Cells

(A) Measurement of mitochondrial movements in H9c2 cells transfected with mitoYFP and pretreated with Tg in a Ca^{2+}-free medium. Kymograms (lower) before (60 s), 8 min after (540 s) H_2O_2, and 1 min (610 s) after $CaCl_2$ additions. Cells were treated with solvent (–) or H_2O_2 where indicated.

(B) MitoYFP-expressing cells were loaded with fura-2 AM and pretreated as in (A). The upper row images show the site of mitochondrial movement (red: positive change, green: negative change between sequential images) at each time point. 340 (red) and 380 nm (green) channels of fura-2 are shown (lower row).

(C) Time courses of motility decay (red) and $[Ca^{2+}]_c$ (black) recorded simultaneously in the same cells. $[Ca^{2+}]_c$-induced motility inhibition is shown at the end of the experiment.

(D) Time courses of motility decay after exposure to varying concentrations of H_2O_2. 100% inhibition was defined by $CaCl_2$ added at the end of the experiment.

(legend continued on next page)

diagram indicating initial motility inhibition with elongation, followed by further deceleration of mitochondria with shortening. Remarkably, X/XO (5 mU/mL) and myxothiazol + oligomycin treatments (used to specifically depolarize $\Delta\Psi_m$ by inhibiting complexes III and V of the oxidative phosphorylation) caused instead partial deceleration with shortening, whereas menadione distinctly triggered partial deceleration with marked elongation. Figure S1J shows that the deceleration caused by specific $\Delta\Psi_m$ depolarization by myxothiazol + oligomycin was far less in extent than the one caused by oxidants, when comparing them at identical potentials (e.g., at −10 mV depolarization). Notably, the myxothiazol + oligomycin-triggered shortening was probably due to swelling rather than fission as it was earlier shown (Gerencser and Nicholls, 2008; Yuan et al., 2007). Figures S1J and S1K indicate that H_2O_2- and menadione-induced inhibition of motility preceded $\Delta\Psi_m$ depolarization, when we consider that $\Delta\Psi_p$ was relatively stable in this time period (Figure S1I). Notably, H_2O_2-induced $\Delta\Psi_p$ hyperpolarization may mask a small extent of $\Delta\Psi_m$ depolarization, but this was not the case for menadione. In contrast, the start of a gradual $\Delta\Psi_{m+p}$ depolarization preceded shortening of mitochondria. Altogether, the different velocity-length temporal tracks triggered by the different oxidants follow independent trends, supporting the idea that the effectors modulating motility and mitochondrial fusion-fission are distinct molecular entities.

H_2O_2-Induced Mitochondrial Motility Inhibition Is Dose Dependent, Is Not Mediated by Ca^{2+}, and Spares Other Organelles

To find out whether the ROS sensitivity of motility was a general cell mechanism and how it was mediated, we used H9c2 myoblasts because mitochondrial motility and its regulation by Ca^{2+} have been studied in this model. Cells were transfected with mitoYFP, and mitochondrial movement response to H_2O_2 addition was represented as kymograms in Figure S2A. The number of movement events significantly diminished 10 min after 200 μM H_2O_2 addition and drastically dropped down at 20 min (Figure S2B), reproducing what was observed in rat hippocampal neurons.

To check the possibility that an ROS-induced $[Ca^{2+}]_c$ rise was the inducer of the motility decay, we next employed Ca^{2+}-depleted H9c2 cells. Cells were pretreated with thapsigargin (Tg; 2 μM), an endoplasmic reticulum (ER)/sarcoplasmic reticulum (SR) Ca^{2+}-ATPase inhibitor, in a Ca^{2+}-free extracellular medium to prevent intracellular Ca^{2+} mobilization and the ensuing Ca^{2+} entry. In these conditions, addition of 100 μM H_2O_2 inhibited motility of mitochondria, which appeared almost all completely immobile after 8 min (540 s of time-lapse recording) as shown by the kymograms in Figure 2A. As expected, addition of 4 mM $CaCl_2$ at the end of the run (610 s) resulted in full inhibition of movements. The inhibitory effect of H_2O_2 on mitochondrial transport in Ca^{2+}-depleted conditions was also confirmed using the photoactivatable fluorescent protein technology (Eisner et al., 2014; Liu et al., 2009; Saotome et al., 2008). Here, the mitochondrial matrix-targeted fluorescent protein is activated in small subregions of the cell, and subsequent time-lapse images show moving of individual mitochondria to other areas (Figures S2C and S2D). In control cells, mitochondria with photoactivated content appeared more and more distant from the photoactivation areas (see images of 540 and 720 s), whereas in cells treated with 100 μM H_2O_2, they remained confined to the photoactivation areas (Figure S2C). Furthermore, when the photoactivated fluorescence was plotted for the photoactivation areas, the time-dependent fluorescence decay was suppressed in H_2O_2-pretreated cells (Figure S2D). Thus, 100 μM H_2O_2 inhibited mitochondrial transport in Ca^{2+}-depleted conditions.

To confirm that no $[Ca^{2+}]_c$ change was caused by H_2O_2, we also loaded cells with fura-2-acetoxymethyl ester (fura-2 AM). Moving mitochondria are shown in the mitoYFP image as red and green pixels in which fluorescence between sequential images (12 s interval) was changing over an empirically determined threshold (Saotome et al., 2008; Yi et al., 2004). The number of red and green pixels progressively decreased by H_2O_2 (100 μM) without any change in $[Ca^{2+}]_c$ (Figures 2B and 2C). As expected, $CaCl_2$ (4 mM) addition caused a $[Ca^{2+}]_c$ increase and further decreased motility. Thus, H_2O_2-induced mitochondrial motility inhibition is independent of a change in $[Ca^{2+}]_c$. It was also present even at lower concentrations of H_2O_2, with the minimum effective concentration being 25 μM and a dose-dependent trend (200 μM; 68% ± 0.8%, 100 μM; 60% ± 1.3%, 50 μM; 41% ± 1.8%, 25 μM; 30% ± 1.7%, 12.5 μM; 3.6% ± 2%; n = 8–10) (Figures 2D and 2E).

Because ROS exposure can cause broad changes in the cells, we tested whether H_2O_2 also affected the transport of peroxisomes visualized by SKL-DsRed (Figure 2F). As for mitochondrial motility, SKL-DsRed-transfected H9c2 were Ca^{2+} predepleted, and the time lapse was recorded in Ca^{2+}-free extracellular medium. H_2O_2 (100 μM) addition did not affect movements of peroxisomes as shown by kymograms at time point 540 s and by traces of motility decay in Figure 2G. As for mitochondria, addition of 4 mM $CaCl_2$ caused rapid decrease of peroxisomal motility. Thus, H_2O_2 targeted mitochondrial motility without causing a broad organellar transport change.

H_2O_2 can cause membrane damage that leads to cell death. To test whether this happened during the time course of our measurements, we used propidium iodide (PI) exclusion. In H9c2 cells (or MEFs used in some experiments later on), addition of H_2O_2 (100 μM) failed to allow PI entry (Figures S2E and S2F). By contrast, digitonin, a detergent added at the end of the run, caused rapid intracellular accumulation of the dye.

Collectively, these results indicate that H_2O_2-induced targeting of mitochondrial motility is a general cell mechanism and it specifically impairs mitochondria movements, leaving peroxisomal motility or cell membrane integrity unaffected at least for the H_2O_2 doses used here. The H_2O_2-induced motility decay takes place independently from $[Ca^{2+}]_c$ change and shows a

(E) Motility inhibition at 8 min after application of H_2O_2.
(F) Measurement of peroxisomal movements in H9c2 cells transfected with SKL-DsRed and pretreated as in (A). Kymograms (lower) before (60 s) and 8 min after (540 s) H_2O_2 addition to H9c2 cells.
(G) Time courses of peroxisomal motility decay (red) and $[Ca^{2+}]_c$ (black) recorded simultaneously in the same cells.

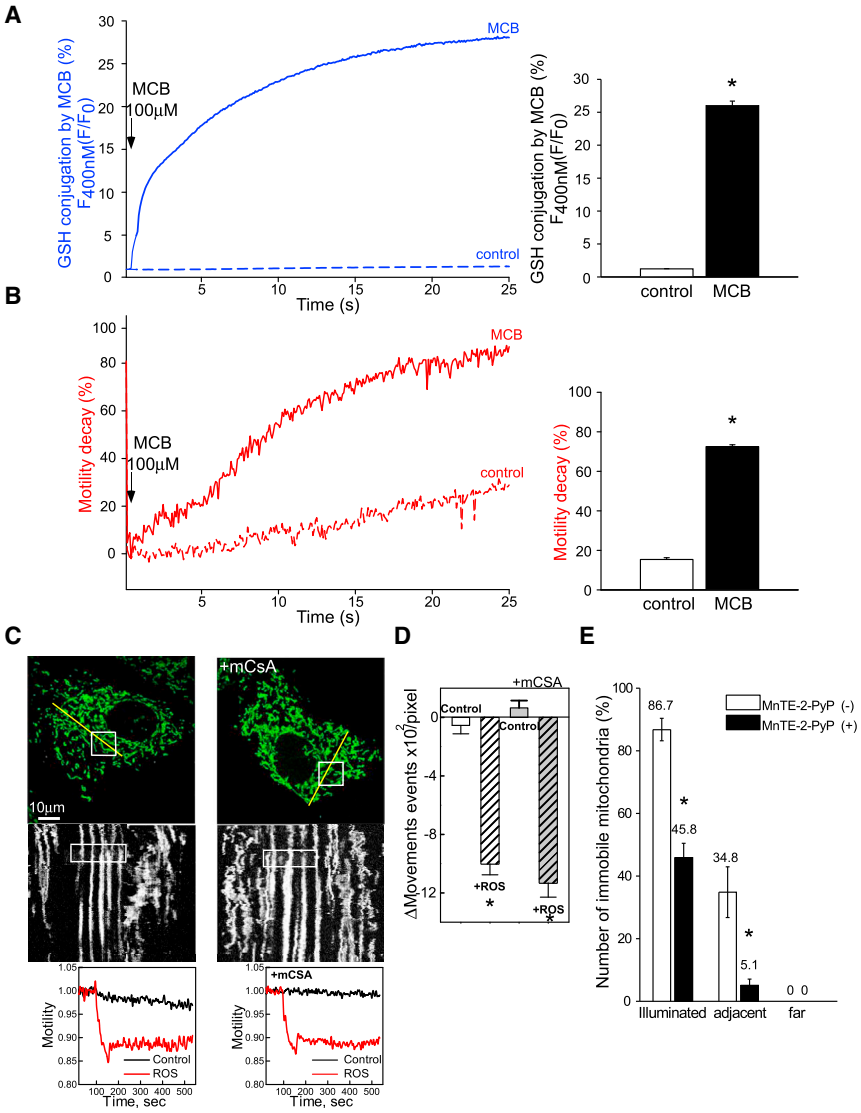

Figure 3. Mitochondrial Motility Is Inhibited by Intracellularly Formed ROS and Is Reversible

(A and B) Simultaneous measurement of GSH conjugation by MCB (A) and motility (mean traces) (B). MitoYFP-expressing H9c2 cells were pretreated with Tg in a Ca^{2+}-free extra-cellular medium (ECM); then MCB was applied. Summarized data at the time point of 15 min after MCB are shown on the right. *$p < 0.01$.

(C) MitoYFP-expressing H9c2 cells were loaded with MitoTrackerRed-CMTRos (MTR) and then pretreated as in (A). Confocal images (upper panel) and respective kymograms (lower) for cells untreated or treated with mCsA (right) are shown. Photoillumination was applied to the boxed area to induce intracellular ROS formation. Time courses of motility for control (black) and photoilluminated (red) are shown normalized to the baseline.

(D) Mitochondrial motility shown as change in the number of recorded events, corresponding to (C). *$p < 0.02$ versus control.

(E) Numbers of immobile mitochondria at the photoilluminated, adjacent, and far areas of the cell. MitoYFP-expressing H9c2 cells were loaded and preincubated as in (C). Immobile mitochondria were counted 5 min after photoillumination in the absence (white bars) and presence of MnTE-2-PyP (black bars). *$p < 0.05$ versus 5 min.

dose-response relationship with the lowest effective concentration of 25 μM.

Endogenous ROS Induce a Decrease in Mitochondrial Motility

Next, effects of endogenously produced ROS were studied first by dampening the antioxidant defense. In hippocampal neurons, glutathione depletion by ethacrynic acid (Vesce et al., 2005), CDNB (Figure 1I), or monochlorobimane (MCB; Figure S1F) reduced mitochondrial motility similarly to oxidants. These findings were recapitulated in mitoYFP-expressing H9c2 cells. MCB becomes fluorescent when it conjugates with glutathione (GSH) in the cells (MCB F/F_0; 26.0 ± 0.7 versus 1.2 ± 0.0 of control; $p < 0.01$; Figure 3A); however, because GSH is major natural scavenger of H_2O_2, the formation of intracellular MCB-GSH rapidly depletes GSH, resulting in an increase in intracellular ROS (Vesce et al., 2005). Upon MCB-GSH conjugation, a significant motility inhibition was observed (72.5% ± 0.9% versus 15.4% ± 0.9% of control; n = 7; $p < 0.01$; Figure 3B). Thus, an intracellular ROS source could reproduce the inhibitory effect on motility observed by externally administering H_2O_2.

To test whether mitochondrial motility was affected even when intracellular ROS were restricted to a small area of the cell, we loaded mitoYFP-expressing H9c2 cells with MitoTracker Red-CMXRos (MTR) and used photoillumination to generate localized intracellular ROS elevation (Figure 3C). Kymograms and plots of motility show a rapid and drastic effect on motility in the area of photoillumination (Figure 3D). To test whether photoillumination per se was exerting an inhibitory effect on motility, we counted the number of immobile mitochondria also in the adjacent area of the cell (Figure 3E). In the photoilluminated area, the number of immobile mitochondria was increased to 86.7%. In the area adjacent to the site of ROS generation, inhibitory effect was still present, even if with a lesser extent (34.8%). As a control, immobile mitochondria were counted in an area far away from the photoilluminated one, and no inhibition of mitochondrial motility was observed (Figure 3E). To further validate the role of ROS in photoillumination-induced motility inhibition, we pre-incubated cells with a scavenger, Mn(III) tetrakis (*N*-ethylpyridinium-2-yl) porphyrin (MnTE-2-PyP) (Figure 3E). Notably, MnTE-2-PyP is a superoxide dismutase mimetic and thus converts $O_2\bullet^-$ to H_2O_2. H_2O_2 is then more efficiently eliminated by the GSH-dependent mechanisms than $O_2\bullet^-$ (Jezek and Hlavatá, 2005). The superoxide dismutase

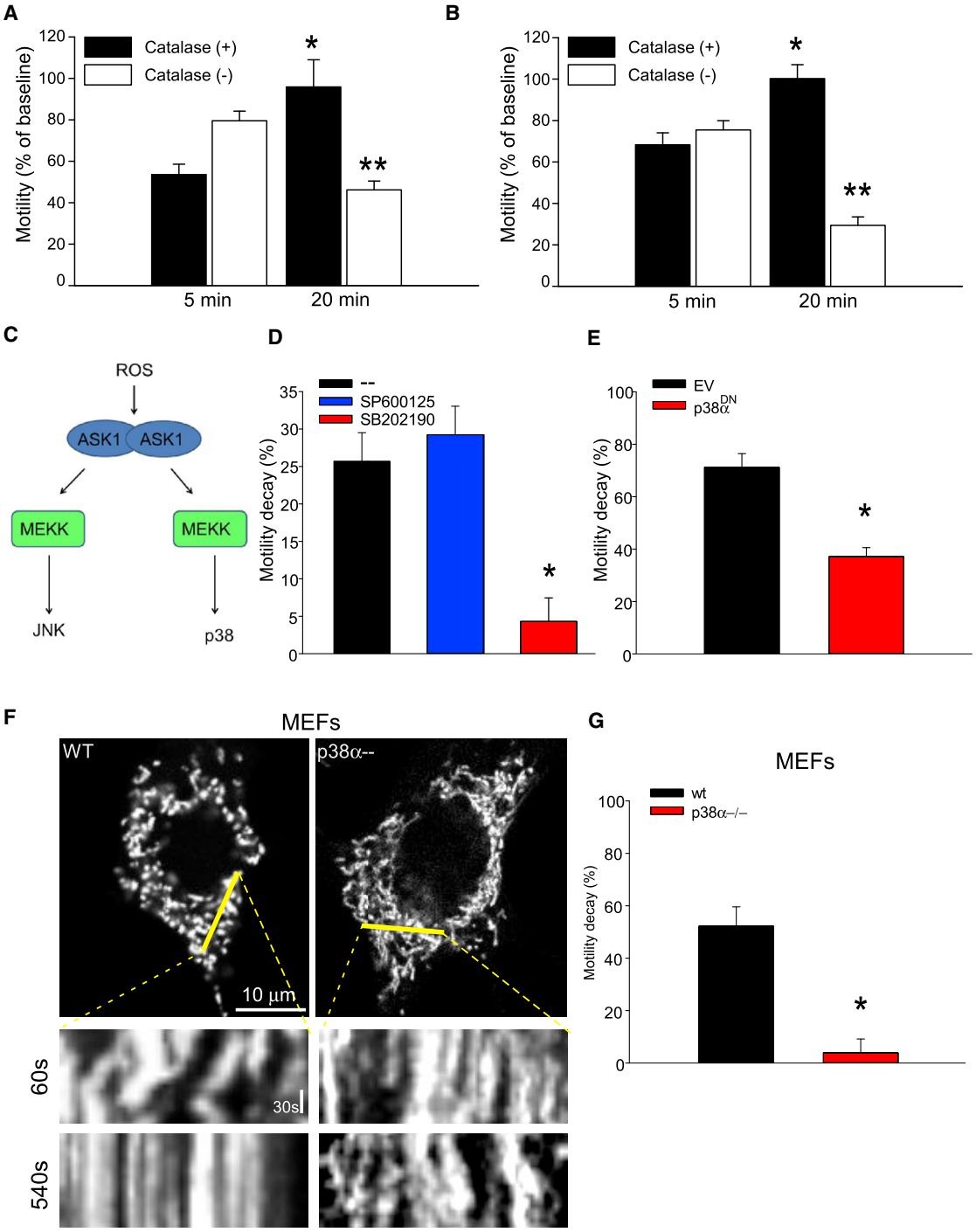

Figure 4. Mitochondrial Motility Inhibition by H_2O_2 Is p38α Mediated (See Also Figure S4)

(A and B) MitoYFP-expressing H9c2 cells were pretreated with Tg in a Ca^{2+}-free ECM; then H_2O_2 was applied in the presence (A) or absence of CsA (B). Motility is shown at 5 and 20 min exposure of H_2O_2 (white bars). H_2O_2 was eliminated by replacing it for catalase (black bars) at 5 min; then the recovery of motility was monitored. *$p < 0.01$ versus 5 min, **$p < 0.01$ versus catalase (+) 20 min.

(C) Graphic representation of ROS-mediated activation of MEK kinases JNK and p38.

(D) Motility decay (calculated as Δ between H_2O_2-treated and untreated cells) at the time point of 3 min after H_2O_2 addition to H9c2 cells. Where indicated, cells were pretreated with SP600125 or SB202190 for 20 min. Unexpectedly, these inhibitors alone caused some decrease in motility (46% ± 2% for SP600125 and 29% ± 3% for SB202190 versus 5% ± 1% untreated cells), indicating that the treated cells became frail and sensitive to imaging conditions. Nevertheless, H_2O_2

(legend continued on next page)

mimetic resulted in attenuation of the photoillumination-induced motility inhibition, with a decrease in the number of immobile mitochondria of almost half of non-treated cells in the photoilluminated area and also in the adjacent area (from 34.5% to 5.1%). Thus, when ROS is produced in a cellular subregion, the motility inhibition is also spatially confined, suggesting that ROS can serve as a local factor in the control of motility.

Neither Mitochondrial PTP Opening nor $\Delta\Psi_m$ Loss Is Required for H_2O_2-Induced Mitochondrial Motility Inhibition

In mammalian cells, directional mitochondrial movements usually take place along microtubules. We therefore investigated whether ROS affected the spatial organization of mitochondria relative to microtubules. In Figure S3A, the confocal images of mitoDsRed and tubulin GFP co-transfected cells revealed that H_2O_2 did not evoke any change in the spatial relationship between mitochondria and microtubules (Figure S3A).

A main mitochondrial target of oxidative stress is the PTP, the opening of which commonly causes mitochondrial dysfunction (Rasola and Bernardi, 2011). Therefore, next it was investigated whether PTP is involved in the ROS-induced motility inhibition. Pre-incubation with the selective PTP inhibitor Me-Val-CSA (mCsA; 5 μM) did not suppress the ROS-dependent mitochondrial motility inhibition (Figures 3C, right panel, and 3D). The broad PTP/calcineurin inhibitor cyclosporine A (CsA) was also applied to Ca^{2+}-depleted cells, and the H_2O_2-induced motility decay was evaluated (Figures S3B and S3C). CsA did not alter the H_2O_2-induced motility inhibition (64.8% ± 1.3% H_2O_2 alone versus 60.9% ± 1.3% of H_2O_2+CsA; n = 37; Figure 3E), confirming that PTP opening was not involved in the phenomenon.

In hippocampal neurons, H_2O_2 and menadione inhibited motility before loss of $\Delta\Psi_m$, and in a greater extent than specific discharging of $\Delta\Psi_m$ did. To further test the relationship between H_2O_2-induced motility inhibition and depolarization, we measured $\Delta\Psi_m$ in Ca^{2+}-depleted H9c2 cells. H_2O_2 did not alter $\Delta\Psi_m$, at least when the motility inhibition became apparent (Figure S3D). In FCCP- and oligomycin-treated cells, dissipation of $\Delta\Psi_m$ was gradually followed by the loss of motility, reflecting the slower kinetic of cytoplasmic ATP depletion (Yi et al., 2004) (Figure S3E). However, even during the uncoupler-induced depolarization, H_2O_2 caused further inhibition in motility (79.4% ± 1.3% versus 62.4% ± 1.2% of control; n = 21; $p < 0.01$; lower plot in Figure S3E), supporting that H_2O_2 suppressed motility independent of $\Delta\Psi_m$ loss.

H_2O_2-Induced Mitochondrial Motility Inhibition Is a Reversible Process

Mitigation of endogenous H_2O_2 was increasing mitochondrial motility in neurons where *N*-acetyl-cysteine was applied, resulting in increased mitochondrial velocities after 40 min (Figure 1I). To further assess the effects of antioxidants on H_2O_2-induced mitochondrial motility inhibition in H9c2 cells, we incubated the Ca^{2+}-depleted cells with H_2O_2, and after the mitochondrial motility inhibition was documented (5 min), the extracellular H_2O_2 was eliminated by catalase (2,500 IU) and motility was reassessed at 20 min. As shown in Figure 4A, catalase treatment reversed H_2O_2-induced motility decrease (96.4% ± 5.5% of motility in treated versus 78.4% ± 4.4% in untreated). Again, treatment with CsA has no effect on the motility inhibition and its reversibility (Figure 4B), arguing against a role of PTP activation in the process.

p38α Is Required for the H_2O_2-Induced Mitochondrial Motility Inhibition

H_2O_2 was reported to induce many changes in protein phosphorylation and activation of signaling factors mediating phosphoregulation like protein kinase C (Shibukawa et al., 2003), protein phosphatase 2A (PP2A) (Rao and Clayton, 2002), and mitogen-activated protein kinases (MAPKs) superfamily through activation of ASK1 MAP3 kinase (Figure 4C) (Ichijo et al., 1997; Saitoh et al., 1998). To evaluate whether any of these pathways were involved here, we screened kinase and phosphatase inhibitors for motility regulation in the presence of H_2O_2. Neither okadaic acid (PP1 and PP2A inhibitor) nor staurosporine (PKC inhibitor) was able to influence on motility inhibition by H_2O_2. To selectively inhibit JNK or p38 MAPK kinases, we used SP600125 or SB202190 in a Ca^{2+}-free condition. H_2O_2 was able to decrease motility in both kinase inhibitor untreated and SP600125-treated cells, but it was ineffective when SB202190 was used (Figure 4D), suggesting an involvement of p38.

Four isoforms of p38 exist in mammals (α, β, δ, and γ). In the heart, all four isoforms are present (Dingar et al., 2010). However, in the brain and many other tissues, only p38α and p38β are expressed (Jiang et al., 1996; Stein et al., 1997). Interestingly, p38 phosphorylation has recently been implied in the regulation of ER-mitochondria associations and motility (Li et al., 2015), and activation of p38α inhibits anterograde fast axonal transport upon expression of a pathogenic mutation of superoxide dismutase 1 (SOD1) (Morfini et al., 2013). To test whether isoform α could play a role in motility regulation, we transfected H9c2 with a dominant-negative mutant of p38α ($p38\alpha^{DN}$), in which Thr180 and Tyr182 residues were mutated to prevent phosphorylation and activation of the MAPK. Dominant-negative interference with p38α also rendered mitochondrial motility gradually declining in our recording conditions (21% ± 3% of motility decay; Figure S2A). H_2O_2 suppressed the remaining motility to a smaller extent in $p38\alpha^{DN}$-expressing cells than in cells transfected with empty vector (EV; Figure 4E).

was able to decrease motility in both kinase inhibitor untreated and SP600125-treated cells, but it was ineffective when SB202190 was used (% of motility decay of 25 ± 4, 29 ± 4 and 4 ± 3, respectively). *$p < 0.002$.

(E) Motility decay (calculated as in D) at 8 min after H_2O_2 addition (black bar) to H9c2 cells transfected with empty vector (EV) or dominant-negative mutant of p38α ($p38\alpha^{DN}$) as indicated. *$p < 0.002$.

(F) Measurement of mitochondrial movements in wild-type (WT) and *p38α knockout* ($p38\alpha^{-/-}$) MEFs transfected with mitoYFP. Kymograms (lower) before (60 s) and 8 min after (540 s) H_2O_2 addition.

(G) Motility decay at 8 min after H_2O_2 addition (black bar) to mitoYFP-expressing MEFs as in (F). Motility was calculated as in (D). *$p < 0.006$.

Mitochondrial motility was then assessed in MEFs lacking p38α (p38$\alpha^{-/-}$). MEFs in general showed more resistance to H_2O_2-induced motility inhibition than hippocampal neurons or H9c2 cells: to achieve a motility decay of 52.2% ± 7.3% at time point of 8 min, we increased the H_2O_2 concentration from 100 to 200 μM. Addition of the same dose of H_2O_2 to p38$\alpha^{-/-}$ MEFs did not cause a decrease of localized mitochondrial movements (Figure 4F) or general mitochondrial motility inhibition (Figure 4G), confirming that p38α is required for the H_2O_2-induced motility arrest.

The Motor Adaptor Complex Is Essential for Mediating the H_2O_2-Induced Mitochondrial Motility Decay

Mitochondrial movements along microtubules and microfilaments are achieved through an adaptor complex (containing Miro1/2 and Trak1/2) and motor proteins (kinesins, dyneins, and myosins). Because the spatial relationship between mitochondria and microtubules is not affected by H_2O_2 (Figure 2G), we reasoned that the activity of one of these two components could be the target of p38 for achieving ROS-induced inhibition of motility. Kinesin KIF5C has been already described as a target of p38 (Morfini et al., 2013): phosphorylation of its serine residue in position 176 regulates cargo transport by promoting disengagement of the motor from microtubule tracks (Padzik et al., 2016). Kif5B, one of the kinesins responsible for movements of mitochondria (Tanaka et al., 1998), together with Kif1B and KLP (Nangaku et al., 1994; Tanaka et al., 2011), belongs to the same kinesin family as Kif5C (Kanai et al., 2000). Serine 176 is conserved between KIF5C and KIF5B, and is also found in KIF1B (Figure S4C). We therefore created a phospho-resistant mutant of KIF5B by mutagenizing residue 176 to alanine (KIF5B^{S176A}) and used it to transfect H9c2 cells (Figure S4D). After exposure to H_2O_2, H9c2 expressing the phospho-resistant mutant of KIF5B exhibited approximately the same percentage of motility decay documented in control cells (55.7% ± 2% for KIF5B^{S176A} and 60.3% ± 2% for EV-transfected cells; Figure S4E). Therefore, expression of phospho-resistant KIF5B^{S176A} was unable to prevent mitochondrial motility inhibition exerted by H_2O_2.

This kinesin in combination with the FRB-FKBP drug-inducible heterodimer was then employed to determine the involvement of Miro/Trak protein complex in the effect exerted by H_2O_2. HA-KIF5B (1-807)-*FRB*, the truncated KIF5B lacking its tail domain, which is known to be constitutively active without interference of regulatory pathways (Kapitein et al., 2010), was fused to FRB and was co-expressed with TOM20-mCherry-FKBP (Chung et al., 2016). Addition of rapalog causes heterodimerization between adjacent FRB and FKBP domains to directly connect kinesin motor proteins to mitochondria. The rearrangement of mitochondrial distribution upon rapalog addition is shown in Figure 5A: mitochondria initially accumulated around the nucleus (150 s) aligned with the microtubular tracks (240 s; see also Figure S4F), where Kif5B is probably anchored, and then move to the peripheral tips of the cell, where they form aggregates (600 s, arrowheads, lower right panel). Cells untreated with rapalog did not show any change in the mitochondrial distribution during the same time (Figure 5A, upper panel).

To assess whether the rapalog-induced anchoring to Kif5B was affecting motility, we quantified the amount of moving mitochondria (represented as red and green pixels, Figure 5B). Expression of the anchor components, in the absence of rapalog, did not substantially change it (Figure 5B, first row). In the same condition, H_2O_2 caused a decrease in mitochondrial motility (second row). However, when mitochondria were directly anchored to KIF5B, H_2O_2 was unable to induce a decrease in the motility (Figures 5B, last two rows, 5C, and 5D). Mean traces of the motility decay for the conditions described above are shown in Figure 5C. These data suggest that H_2O_2 targets the motor adaptor complex via p38α to suppress mitochondrial movements.

DISCUSSION

This work provides evidence for the control of mitochondrial motility by ROS, through a p38α-dependent pathway and the adaptor complex that anchors mitochondria to the microtubular motor proteins. Both external and internal sources of ROS cause a decrease in mitochondrial motility in rat hippocampal neurons and H9c2 cells. This is attained by small amounts of ROS like 25 μM H_2O_2 and is rapidly reversible. ROS can stop mitochondrial movements independent of $[Ca^{2+}]_c$, a well-known mitochondrial motility regulator, and of $\Delta\psi_m$. Furthermore, ROS-induced mitochondrial dysfunction or PTP opening is not involved in H_2O_2-induced motility decay. Based on genetic and pharmacological evidence, ROS inhibition of mitochondrial motility requires a p38α pathway and seems to target specifically the adaptor complex that links mitochondria to the microtubular motor proteins.

Due to their polarized and complex functional and structural organization, neurons need to distribute mitochondria in neurites, to reach areas where their metabolic activity is required (like synapses) and to easily drive their engulfment and elimination and replacement when they become dysfunctional during cellular stress. ROS function as intracellular messengers in long-term potentiation but also represent a source of synaptic stress, when their elevation is sustained. We here showed that oxidative stress (H_2O_2, $O_2\cdot^-$, menadione, and GSH depletion) rapidly suppresses mitochondrial velocity in rat hippocampal neurons in a dose-dependent manner. Importantly, inhibition of motility was distinguished from ROS-induced mitochondrial elongation and fragmentation, which are evoked by prolonged/massive ROS exposure. We have studied the mechanism of the motility inhibition (see below) and speculate that a separate ROS-activated pathway engages the mitochondrial fusion-fission proteins likely by posttranslational modification, but establishing this point requires further studies.

To investigate the mechanisms underlying the ROS-induced mitochondrial motility inhibition, we switched to H9c2 cells that we had extensively used in previous works to dissect mitochondrial dynamics. ROS likely target functionally relevant SH groups in proteins, but the number of candidate proteins is high. We considered three potential mechanisms to decrease mitochondria motility in response to ROS. First, ROS could induce a rise in $[Ca^{2+}]_c$ through sensitization to threshold concentrations of inositol-1,4,5-trisphosphate (IP_3)-linked agonists (Booth et al.,

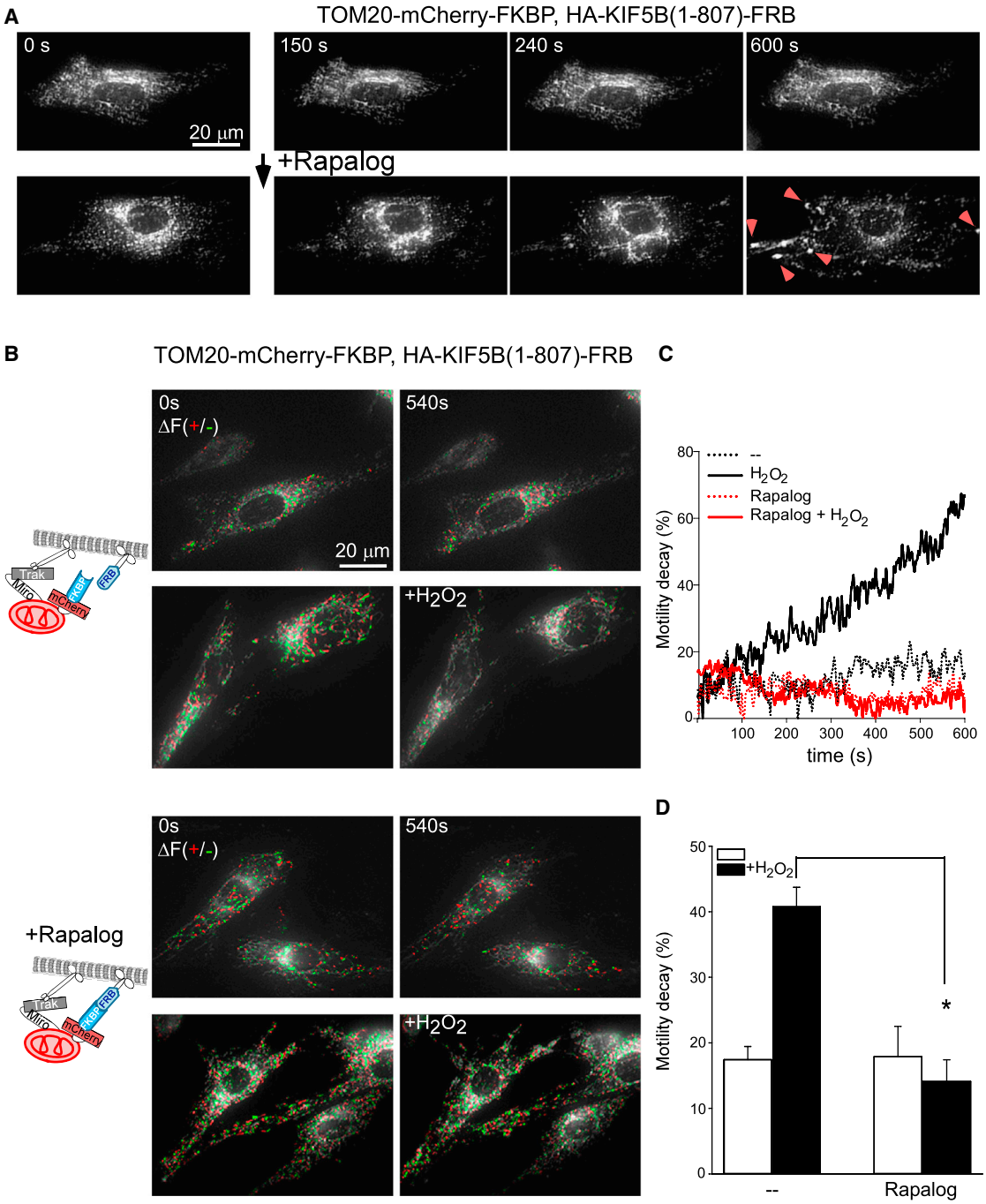

Figure 5. The Adaptor Complex Is Essential for Mediating the H_2O_2-Induced Mitochondrial Motility Decay

(A) Confocal images of H9c2 cells expressing TOM20-mCherry-FKBP and HA-KIF5B (1-807)-FRB show the distribution of mitochondria (at 0, 150, 240, and 600 s) with (lower) or without (w/o) (upper) rapalog treatment. Note the rapalog-induced marked conglomeration of mitochondria at the distal tips of the cell at 600 s (arrowheads).

(B) Confocal images show motility in of H9c2 cells overexpressing mito-kinesin linker at times 0 and 540 s. Where indicated, rapalog and/or H_2O_2 was applied at 60 s.

(C) Mean traces of motility decay with (solid lines) or w/o (dotted lines) H_2O_2 addition in the presence (red) or absence (black) of rapalog. Treatments were applied at 60 s. Schematic representations of adaptor motor complex and the mito-kinesin linker before and after rapalog-induced heterodimerization are shown.

(D) Motility decay 8 min (540 s) after H_2O_2 (black bar) and rapalog addition. Experiments were as in (C). *$p < 0.001$.

2016) and through modulation of ER or plasma membrane Ca^{2+} transport mechanisms (Bootman et al., 1997; Csordás and Hajnóczky, 2009; Prosser et al., 2011). However, we here showed that Ca^{2+} pre-depleted cells also underwent motility decay upon addition of H_2O_2 without any rise in $[Ca^{2+}]_c$. Thus, in our case, ROS can inhibit motility independently of $[Ca^{2+}]_c$. Conversely, Ca^{2+}-induced motility arrest could involve ROS. Ca^{2+} can increase ROS generation by enhancing tricarboxylic acid cycle and making the mitochondrial redox centers more reduced (Brand, 2016; Hansford and Zorov, 1998; McCormack and Denton, 1993) and by opening the PTP (Vercesi et al., 1997). However, we have shown that Ca^{2+} does not have to enter mitochondria to control motility (Yi et al., 2004). Ca^{2+} could also act on extramitochondrial enzymes like NADPH oxidase, cytochrome P450, xanthine oxidase, cyclooxygenase, and lipoxygenase to enhance ROS (Kevin et al., 2003; Sauer et al., 2001), or on mitochondria externally, by activating reductive equivalent shuttles (Orr et al., 2012). However, the mitochondrial motility inhibition closely follows the $[Ca^{2+}]_c$ rise and is dependent on the EF-hands of Miro, indicating a fairly direct interaction of Ca^{2+} with the adaptor/motor complex (MacAskill et al., 2009b; Saotome et al., 2008; Wang and Schwarz, 2009; Yi et al., 2004). Thus, Ca^{2+} and ROS seem to have privileged mechanisms to target mitochondrial motility, but they can also engage each other to regulate motility.

The next potential candidates to mediate ROS-induced mitochondrial motility inhibition were PTP opening and loss of the mitochondrial membrane potential, because they have been shown to be outcomes of oxidative stress (De Vos et al., 2007; Rasola and Bernardi, 2011). But neither PTP inhibition nor predissipation of the membrane potential prevented the H_2O_2-induced motility inhibition.

Lastly, we considered that many effects of ROS are relayed to changes in protein phosphorylation, and we employed first a pharmacological approach to test the possible involvement of protein kinases and phosphatases. From the drugs tested, only SB202190, an inhibitor of p38, attenuated the motility decay caused by H_2O_2. However, SB202190 has been reported to stimulate ruthenium red-sensitive mitochondrial Ca^{2+} uptake in both p38-dependent and -independent manners (Montero et al., 2002; Szanda et al., 2008). Therefore, we used two independent genetic models to verify whether p38α was involved in the process of H_2O_2-induced mitochondrial motility inhibition: (1) H9c2 cells were transfected with p38α^{DN}, and (2) MEFs ablated of p38α were challenged with H_2O_2. Both sets of experiments demonstrated that p38α is required for the H_2O_2-induced motility decrease. In a previous work, SB202190-induced motility inhibition was ascribed to an increased mitochondrial Ca^{2+} uptake (Chang et al., 2011). However, we documented the H_2O_2-induced motility decrease in Tg-pretreated cells incubated in the absence of extracellular Ca^{2+}, where no mitochondrial Ca^{2+} uptake could occur. In addition, H_2O_2 was unable to induce inhibition when p38 was targeted, suggesting that p38 activation in response to ROS might mediate the inhibition of the organellar movements.

When mitochondria were forced to directly associate to a motor protein through a drug-induced FRB-FKBP tether, the effect of H_2O_2 on motility was prevented, suggesting that ROS target the adaptor complex. Phosphorylation of mitochondrial and cytosolic substrates has been recently proposed as the mechanism that drives redistribution of mitochondria during mitosis (Chung et al., 2016). In that study, phosphorylation drives detachment of mitochondria + adaptor from motor protein. However, we did not document a change in the association of mitochondria to microtubules upon ROS elevation. This observation is also an argument against switching of mitochondria to microfilaments or intermediate filaments, which also support mitochondrial positioning (Kuznetsov et al., 1992; Nekrasova et al., 2011; Pathak et al., 2010; Schwarz and Leube, 2016). Alternative explanations are that the adaptor might respond to ROS and p38α activation by relaying an inhibitory signal to the motor proteins or by binding to less active motor proteins.

Mitochondrial motility inhibition is induced by physiologically relevant doses of H_2O_2 and is rapidly reversed by removal of H_2O_2. This supports the idea that ROS might work as a physiological regulator of mitochondrial distribution, temporally decelerating the organelles when and where it is required. This process may enable to recruit additional mitochondria at the site of ROS elevation, and serve both ROS scavenging and propagation of ROS production, which may have relevance in pathophysiological conditions. Finally, in line with recent findings on ROS/Ca^{2+} communication at mitochondria-ER contact sites (Booth et al., 2016) and on the involvement of mitochondrial respiratory complex I- and III-originated ROS in ER-stress-induced caspase activation (Brand et al., 2016), a Ca^{2+}-induced rise in mitochondrial ROS could serve as a signal to stop mitochondria in proximity to ER to establish new contact sites to serve as signaling modulators. Thus, our findings offer some clues relevant for mitochondrial quality control and for both cell survival and death signaling.

In the final phase of the writing of this manuscript, a paper came out on oxidative stress (paraquat and H_2O_2)-induced motility inhibition in fly neurons (Liao et al., 2017). Thus, ROS control motility both in fly and in mammalian cells, although in fly, the ROS effect seems to be mediated via $[Ca^{2+}]_c$ elevation, whereas in mammalian cells, ROS can engage robust motility inhibition even independent of Ca^{2+}. Liao et al. (2017) speculated that elevated $[Ca^{2+}]_c$ acts through Miro1, a mitochondrial anchor for motors, and we provided experimental evidence that the motor adaptor complex is needed for the inhibitory effect of ROS. Interestingly, in fly, JNK was also implicated in the motility inhibition, whereas in mammalian cells, p38α is required and JNK is dispensable. p38α is present in fly but was not investigated by Liao et al. (2017). From the two studies, an evolutionarily conserved ROS phenotype emerges in motility that uses species-specific underlying mechanisms to target the mitochondrial motor adaptor complex.

EXPERIMENTAL PROCEDURES

Detailed protocols are available in the Supplemental Experimental Procedures.

Cell Culture, Loading, and Transfection

Primary hippocampal neurons, H9c2 myoblast cells, and MEF cells were prepared, transfected, and treated as in Gerencser and Nicholls (2008), Nguyen et al. (2014), and Yi et al., (2004). All procedures involving rats were carried

out according to the local animal care and use committee (Egyetemi Allatkiserleti Bizottsag) guidelines.

Fluorescence and Confocal Imaging

Time-lapse fluorescence microscopy of hippocampal neurons was performed on an Olympus IX81, while measurements $[Ca^{2+}]_c$ and/or mitochondrial motility in H9c2 and MEFs were carried out on an Olympus IX70 with UAPO 40× oil 1.3 NA lens. Confocal imaging was performed using a Radiance 2100 (Bio-Rad).

Evaluation of Mitochondrial Motility

Mitochondrial velocities were measured as optical flow (Gerencser and Nicholls, 2008), whereas motility in H9c2 cells and MEFs was evaluated as described previously (Saotome et al., 2008; Yi et al., 2004).

Statistical Analysis

All experiments were performed with at least three different preparations. Data are presented mean ± SEM, and significance of difference was calculated by t test unless otherwise indicated. For measurements of mitochondrial velocities in neurons, nine cells were pooled from each preparation, and the results were tested using ANOVA (Dunnett's post hoc test, treatment versus control, independently for the two time points). For measurements of $\Delta\Psi_p$ in neurons, data are % of baseline fluorescence (n = 81, 107, and 70 cells for control, H_2O_2, and menadione, respectively). For measurements of mitochondrial motility in H9c2 cells and MEFs for each condition, 7–10 cells/preparation were evaluated.

SUPPLEMENTAL INFORMATION

Supplemental Information includes Supplemental Experimental Procedures and four figures and can be found with this article online at https://doi.org/10.1016/j.celrep.2017.10.060.

AUTHOR CONTRIBUTIONS

V.D., A.A.G., M.S., and G.H. conceived the ideas; V.D., A.A.G., M.S., and S.D. performed experiments; V.D., A.A.G., M.S., and G.H. wrote the manuscript.

ACKNOWLEDGMENTS

We thank Mr. David Weaver for the assistance with confocal microscopy and coding ImageJ macros for motility analysis. This work was supported by NIH grants DK51526 (to G.H.) and PL1 AG032118 (to A.A.G.). A.A.G. declares financial interest in Image Analyst Software.

Received: June 6, 2017
Revised: September 18, 2017
Accepted: October 15, 2017
Published: November 7, 2017

REFERENCES

Booth, D.M., Joseph, S.K., and Hajnóczky, G. (2016). Subcellular ROS imaging methods: relevance for the study of calcium signaling. Cell Calcium *60*, 65–73.

Bootman, M., Niggli, E., Berridge, M., and Lipp, P. (1997). Imaging the hierarchical Ca2+ signalling system in HeLa cells. J. Physiol. *499*, 307–314.

Brand, M.D. (2016). Mitochondrial generation of superoxide and hydrogen peroxide as the source of mitochondrial redox signaling. Free Radic. Biol. Med. *100*, 14–31.

Brand, M.D., Goncalves, R.L., Orr, A.L., Vargas, L., Gerencser, A.A., Borch Jensen, M., Wang, Y.T., Melov, S., Turk, C.N., Matzen, J.T., et al. (2016). Suppressors of superoxide-H_2O_2 production at site IQ of mitochondrial complex I protect against stem cell hyperplasia and ischemia-reperfusion injury. Cell Metab. *24*, 582–592.

Brickley, K., Smith, M.J., Beck, M., and Stephenson, F.A. (2005). GRIF-1 and OIP106, members of a novel gene family of coiled-coil domain proteins: association in vivo and in vitro with kinesin. J. Biol. Chem. *280*, 14723–14732.

Brough, D., Schell, M.J., and Irvine, R.F. (2005). Agonist-induced regulation of mitochondrial and endoplasmic reticulum motility. Biochem. J. *392*, 291–297.

Chada, S.R., and Hollenbeck, P.J. (2004). Nerve growth factor signaling regulates motility and docking of axonal mitochondria. Curr. Biol. *14*, 1272–1276.

Chang, K.T., Niescier, R.F., and Min, K.T. (2011). Mitochondrial matrix Ca2+ as an intrinsic signal regulating mitochondrial motility in axons. Proc. Natl. Acad. Sci. USA *108*, 15456–15461.

Chung, J.Y., Steen, J.A., and Schwarz, T.L. (2016). Phosphorylation-induced motor shedding is required at mitosis for proper distribution and passive inheritance of mitochondria. Cell Rep. *16*, 2142–2155.

Csordás, G., and Hajnóczky, G. (2009). SR/ER-mitochondrial local communication: calcium and ROS. Biochim. Biophys. Acta *1787*, 1352–1362.

Das, S., Hajnóczky, N., Antony, A.N., Csordás, G., Gaspers, L.D., Clemens, D.L., Hoek, J.B., and Hajnóczky, G. (2012). Mitochondrial morphology and dynamics in hepatocytes from normal and ethanol-fed rats. Pflugers Arch. *464*, 101–109.

De Vos, K.J., Chapman, A.L., Tennant, M.E., Manser, C., Tudor, E.L., Lau, K.F., Brownlees, J., Ackerley, S., Shaw, P.J., McLoughlin, D.M., et al. (2007). Familial amyotrophic lateral sclerosis-linked SOD1 mutants perturb fast axonal transport to reduce axonal mitochondria content. Hum. Mol. Genet. *16*, 2720–2728.

Dingar, D., Merlen, C., Grandy, S., Gillis, M.A., Villeneuve, L.R., Mamarbachi, A.M., Fiset, C., and Allen, B.G. (2010). Effect of pressure overload-induced hypertrophy on the expression and localization of p38 MAP kinase isoforms in the mouse heart. Cell. Signal. *22*, 1634–1644.

Eisner, V., Lenaers, G., and Hajnóczky, G. (2014). Mitochondrial fusion is frequent in skeletal muscle and supports excitation-contraction coupling. J. Cell Biol. *205*, 179–195.

Eklöw, L., Thor, H., and Orrenius, S. (1981). Formation and efflux of glutathione disulfide studied in isolated rat hepatocytes. FEBS Lett. *127*, 125–128.

Fang, C., Bourdette, D., and Banker, G. (2012). Oxidative stress inhibits axonal transport: implications for neurodegenerative diseases. Mol. Neurodegener. *7*, 29.

Fransson, S., Ruusala, A., and Aspenström, P. (2006). The atypical Rho GTPases Miro-1 and Miro-2 have essential roles in mitochondrial trafficking. Biochem. Biophys. Res. Commun. *344*, 500–510.

Gerencser, A.A., and Nicholls, D.G. (2008). Measurement of instantaneous velocity vectors of organelle transport: mitochondrial transport and bioenergetics in hippocampal neurons. Biophys. J. *95*, 3079–3099.

Gerencser, A.A., Doczi, J., Töröcsik, B., Bossy-Wetzel, E., and Adam-Vizi, V. (2008). Mitochondrial swelling measurement in situ by optimized spatial filtering: astrocyte-neuron differences. Biophys. J. *95*, 2583–2598.

Glater, E.E., Megeath, L.J., Stowers, R.S., and Schwarz, T.L. (2006). Axonal transport of mitochondria requires milton to recruit kinesin heavy chain and is light chain independent. J. Cell Biol. *173*, 545–557.

Guo, X., Macleod, G.T., Wellington, A., Hu, F., Panchumarthi, S., Schoenfield, M., Marin, L., Charlton, M.P., Atwood, H.L., and Zinsmaier, K.E. (2005). The GTPase dMiro is required for axonal transport of mitochondria to Drosophila synapses. Neuron *47*, 379–393.

Hansford, R.G., and Zorov, D. (1998). Role of mitochondrial calcium transport in the control of substrate oxidation. Mol. Cell. Biochem. *184*, 359–369.

Hirokawa, N., Sato-Yoshitake, R., Kobayashi, N., Pfister, K.K., Bloom, G.S., and Brady, S.T. (1991). Kinesin associates with anterogradely transported membranous organelles in vivo. J. Cell Biol. *114*, 295–302.

Ichijo, H., Nishida, E., Irie, K., ten Dijke, P., Saitoh, M., Moriguchi, T., Takagi, M., Matsumoto, K., Miyazono, K., and Gotoh, Y. (1997). Induction of apoptosis by ASK1, a mammalian MAPKKK that activates SAPK/JNK and p38 signaling pathways. Science *275*, 90–94.

Jezek, P., and Hlavatá, L. (2005). Mitochondria in homeostasis of reactive oxygen species in cell, tissues, and organism. Int. J. Biochem. Cell Biol. *37*, 2478–2503.

Jiang, Y., Chen, C., Li, Z., Guo, W., Gegner, J.A., Lin, S., and Han, J. (1996). Characterization of the structure and function of a new mitogen-activated protein kinase (p38beta). J. Biol. Chem. *271*, 17920–17926.

Kanai, Y., Okada, Y., Tanaka, Y., Harada, A., Terada, S., and Hirokawa, N. (2000). KIF5C, a novel neuronal kinesin enriched in motor neurons. J. Neurosci. *20*, 6374–6384.

Kapitein, L.C., Schlager, M.A., van der Zwan, W.A., Wulf, P.S., Keijzer, N., and Hoogenraad, C.C. (2010). Probing intracellular motor protein activity using an inducible cargo trafficking assay. Biophys. J. *99*, 2143–2152.

Kevin, L.G., Camara, A.K., Riess, M.L., Novalija, E., and Stowe, D.F. (2003). Ischemic preconditioning alters real-time measure of O2 radicals in intact hearts with ischemia and reperfusion. Am. J. Physiol. Heart Circ. Physiol. *284*, H566–H574.

Kuznetsov, S.A., Langford, G.M., and Weiss, D.G. (1992). Actin-dependent organelle movement in squid axoplasm. Nature *356*, 722–725.

Li, L., Gao, G., Shankar, J., Joshi, B., Foster, L.J., and Nabi, I.R. (2015). p38 MAP kinase-dependent phosphorylation of the Gp78 E3 ubiquitin ligase controls ER-mitochondria association and mitochondria motility. Mol. Biol. Cell *26*, 3828–3840.

Liao, P.C., Tandarich, L.C., and Hollenbeck, P.J. (2017). ROS regulation of axonal mitochondrial transport is mediated by Ca2+ and JNK in Drosophila. PLoS ONE *12*, e0178105.

Liu, X., Weaver, D., Shirihai, O., and Hajnóczky, G. (2009). Mitochondrial 'kiss-and-run': interplay between mitochondrial motility and fusion-fission dynamics. EMBO J. *28*, 3074–3089.

MacAskill, A.F., Brickley, K., Stephenson, F.A., and Kittler, J.T. (2009a). GTPase dependent recruitment of Grif-1 by Miro1 regulates mitochondrial trafficking in hippocampal neurons. Mol. Cell. Neurosci. *40*, 301–312.

MacAskill, A.F., Rinholm, J.E., Twelvetrees, A.E., Arancibia-Carcamo, I.L., Muir, J., Fransson, A., Aspenstrom, P., Attwell, D., and Kittler, J.T. (2009b). Miro1 is a calcium sensor for glutamate receptor-dependent localization of mitochondria at synapses. Neuron *61*, 541–555.

Magrané, J., Cortez, C., Gan, W.B., and Manfredi, G. (2014). Abnormal mitochondrial transport and morphology are common pathological denominators in SOD1 and TDP43 ALS mouse models. Hum. Mol. Genet. *23*, 1413–1424.

Mattson, M.P., Gleichmann, M., and Cheng, A. (2008). Mitochondria in neuroplasticity and neurological disorders. Neuron *60*, 748–766.

McCormack, J.G., and Denton, R.M. (1993). The role of intramitochondrial Ca2+ in the regulation of oxidative phosphorylation in mammalian tissues. Biochem. Soc. Trans. *21*, 793–799.

Miller, K.E., and Sheetz, M.P. (2004). Axonal mitochondrial transport and potential are correlated. J. Cell Sci. *117*, 2791–2804.

Montero, M., Lobaton, C.D., Moreno, A., and Alvarez, J. (2002). A novel regulatory mechanism of the mitochondrial Ca2+ uniporter revealed by the p38 mitogen-activated protein kinase inhibitor SB202190. FASEB J. *16*, 1955–1957.

Morfini, G.A., Bosco, D.A., Brown, H., Gatto, R., Kaminska, A., Song, Y., Molla, L., Baker, L., Marangoni, M.N., Berth, S., et al. (2013). Inhibition of fast axonal transport by pathogenic SOD1 involves activation of p38 MAP kinase. PLoS ONE *8*, e65235.

Mouli, P.K., Twig, G., and Shirihai, O.S. (2009). Frequency and selectivity of mitochondrial fusion are key to its quality maintenance function. Biophys. J. *96*, 3509–3518.

Nangaku, M., Sato-Yoshitake, R., Okada, Y., Noda, Y., Takemura, R., Yamazaki, H., and Hirokawa, N. (1994). KIF1B, a novel microtubule plus end-directed monomeric motor protein for transport of mitochondria. Cell *79*, 1209–1220.

Nekrasova, O.E., Mendez, M.G., Chernoivanenko, I.S., Tyurin-Kuzmin, P.A., Kuczmarski, E.R., Gelfand, V.I., Goldman, R.D., and Minin, A.A. (2011). Vimentin intermediate filaments modulate the motility of mitochondria. Mol. Biol. Cell *22*, 2282–2289.

Nguyen, T.T., Oh, S.S., Weaver, D., Lewandowska, A., Maxfield, D., Schuler, M.H., Smith, N.K., Macfarlane, J., Saunders, G., Palmer, C.A., et al. (2014). Loss of Miro1-directed mitochondrial movement results in a novel murine model for neuron disease. Proc. Natl. Acad. Sci. USA *111*, E3631–E3640.

Nicholls, D.G. (2006). Simultaneous monitoring of ionophore- and inhibitor-mediated plasma and mitochondrial membrane potential changes in cultured neurons. J. Biol. Chem. *281*, 14864–14874.

Orr, A.L., Quinlan, C.L., Perevoshchikova, I.V., and Brand, M.D. (2012). A refined analysis of superoxide production by mitochondrial sn-glycerol 3-phosphate dehydrogenase. J. Biol. Chem. *287*, 42921–42935.

Padzik, A., Deshpande, P., Hollos, P., Franker, M., Rannikko, E.H., Cai, D., Prus, P., Mågård, M., Westerlund, N., Verhey, K.J., et al. (2016). KIF5C S176 phosphorylation regulates microtubule binding and transport efficiency in mammalian neurons. Front. Cell. Neurosci. *10*, 57.

Pathak, D., Sepp, K.J., and Hollenbeck, P.J. (2010). Evidence that myosin activity opposes microtubule-based axonal transport of mitochondria. J. Neurosci. *30*, 8984–8992.

Prosser, B.L., Hernández-Ochoa, E.O., and Schneider, M.F. (2011). S100A1 and calmodulin regulation of ryanodine receptor in striated muscle. Cell Calcium *50*, 323–331.

Rao, R.K., and Clayton, L.W. (2002). Regulation of protein phosphatase 2A by hydrogen peroxide and glutathionylation. Biochem. Biophys. Res. Commun. *293*, 610–616.

Rasola, A., and Bernardi, P. (2011). Mitochondrial permeability transition in Ca(2+)-dependent apoptosis and necrosis. Cell Calcium *50*, 222–233.

Rintoul, G.L., Filiano, A.J., Brocard, J.B., Kress, G.J., and Reynolds, I.J. (2003). Glutamate decreases mitochondrial size and movement in primary forebrain neurons. J. Neurosci. *23*, 7881–7888.

Saitoh, M., Nishitoh, H., Fujii, M., Takeda, K., Tobiume, K., Sawada, Y., Kawabata, M., Miyazono, K., and Ichijo, H. (1998). Mammalian thioredoxin is a direct inhibitor of apoptosis signal-regulating kinase (ASK) 1. EMBO J. *17*, 2596–2606.

Saotome, M., Safiulina, D., Szabadkai, G., Das, S., Fransson, A., Aspenstrom, P., Rizzuto, R., and Hajnóczky, G. (2008). Bidirectional Ca2+-dependent control of mitochondrial dynamics by the Miro GTPase. Proc. Natl. Acad. Sci. USA *105*, 20728–20733.

Sauer, H., Wartenberg, M., and Hescheler, J. (2001). Reactive oxygen species as intracellular messengers during cell growth and differentiation. Cell. Physiol. Biochem. *11*, 173–186.

Schwarz, N., and Leube, R.E. (2016). Intermediate filaments as organizers of cellular space: how they affect mitochondrial structure and function. Cells *5*, 5.

Shibukawa, Y., Takahashi, M., Laffont, I., Honke, K., and Taniguchi, N. (2003). Down-regulation of hydrogen peroxide-induced PKC delta activation in N-acetylglucosaminyltransferase III-transfected HeLaS3 cells. J. Biol. Chem. *278*, 3197–3203.

Stein, B., Yang, M.X., Young, D.B., Janknecht, R., Hunter, T., Murray, B.W., and Barbosa, M.S. (1997). p38-2, a novel mitogen-activated protein kinase with distinct properties. J. Biol. Chem. *272*, 19509–19517.

Stowers, R.S., Megeath, L.J., Górska-Andrzejak, J., Meinertzhagen, I.A., and Schwarz, T.L. (2002). Axonal transport of mitochondria to synapses depends on milton, a novel Drosophila protein. Neuron *36*, 1063–1077.

Szanda, G., Koncz, P., Rajki, A., and Spät, A. (2008). Participation of p38 MAPK and a novel-type protein kinase C in the control of mitochondrial Ca2+ uptake. Cell Calcium *43*, 250–259.

Tanaka, Y., Kanai, Y., Okada, Y., Nonaka, S., Takeda, S., Harada, A., and Hirokawa, N. (1998). Targeted disruption of mouse conventional kinesin heavy chain, kif5B, results in abnormal perinuclear clustering of mitochondria. Cell *93*, 1147–1158.

Tanaka, K., Sugiura, Y., Ichishita, R., Mihara, K., and Oka, T. (2011). KLP6: a newly identified kinesin that regulates the morphology and transport of mitochondria in neuronal cells. J. Cell Sci. *124*, 2457–2465.

Vanden Berghe, P., Hennig, G.W., and Smith, T.K. (2004). Characteristics of intermittent mitochondrial transport in guinea pig enteric nerve fibers. Am. J. Physiol. Gastrointest. Liver Physiol. *286*, G671–G682.

Verburg, J., and Hollenbeck, P.J. (2008). Mitochondrial membrane potential in axons increases with local nerve growth factor or semaphorin signaling. J. Neurosci. *28*, 8306–8315.

Vercesi, A.E., Kowaltowski, A.J., Grijalba, M.T., Meinicke, A.R., and Castilho, R.F. (1997). The role of reactive oxygen species in mitochondrial permeability transition. Biosci. Rep. *17*, 43–52.

Vesce, S., Jekabsons, M.B., Johnson-Cadwell, L.I., and Nicholls, D.G. (2005). Acute glutathione depletion restricts mitochondrial ATP export in cerebellar granule neurons. J. Biol. Chem. *280*, 38720–38728.

Wang, X., and Schwarz, T.L. (2009). The mechanism of Ca2+ -dependent regulation of kinesin-mediated mitochondrial motility. Cell *136*, 163–174.

Yaffe, M.P. (1999). The machinery of mitochondrial inheritance and behavior. Science *283*, 1493–1497.

Yi, M., Weaver, D., and Hajnóczky, G. (2004). Control of mitochondrial motility and distribution by the calcium signal: a homeostatic circuit. J. Cell Biol. *167*, 661–672.

Yuan, H., Gerencser, A.A., Liot, G., Lipton, S.A., Ellisman, M., Perkins, G.A., and Bossy-Wetzel, E. (2007). Mitochondrial fission is an upstream and required event for bax foci formation in response to nitric oxide in cortical neurons. Cell Death Differ. *14*, 462–471.

Zucker, R.S. (1999). Calcium- and activity-dependent synaptic plasticity. Curr. Opin. Neurobiol. *9*, 305–313.